This manuscript has been accepted for publication in the Philippine Journal of Science. However, despite having been peer-reviewed, the final version of the manuscript is yet to be formally published. Feel free to contact the authors if you have any feedback or comments or if you would like to know more about the study.

*Corresponding Author: advcarrillo@gmail.com; +69612656020

Drivers of changes in shoreline position of two small reef islands in the West Philippine Sea

Anne Drew V. Carrillo [1, 2] *, Mary Rose P. Gabuyo [2], Denise Faye S. Janer [1, 2], Paolo Emanuel Y. Co [2] and Fernando P. Siringan [1,2]

[1] Marine Science Institute, University of the Philippines Diliman, Quezon City, Metro Manila, Philippines

[2] Pag-asa Island Research Station, Kalayaan Island Group, Palawan, Philippines

Keywords: coastal erosion, atoll, reef island, sediment transport, West Philippine Sea

*Corresponding Author: advcarrillo@gmail.com; +69612656020

ABSTRACT

This study examines the variations in the shoreline position of two atoll reef islands in the West Philippine Sea, Pag-asa Island, and Lawak Island, and identifies the influence of potential drivers of erosion. Data from field observations, beach profiling, and Google Earth Pro satellite images from 2004 to 2022 are used to identify shoreline movement for each island. Shoreline change is calculated, and area change is measured for each island. Seasonal changes in shoreline position due to seasonal variations in wind regime are observed in Lawak Island, but not in Pag-asa Island. The lack of seasonal variation in the shorelines of Pag-asa Island are attributed to solid-based structures impeding sediment drift around the island. The overall trend of relative sea-level rise is correlated with the overall erosion and interannual changes in sea level which coincides with interannual variations in area change for both islands. Storm events are also found to lead to erosion and the raising of the island elevation through overwash deposition. The overall changes in shoreline position show that the northern and eastern coasts of Pag-asa Island and Lawak Island, eroded faster than their southern and western coasts, respectively. Such variations are attributed to the overall weakening of Southwest Monsoon winds and more consistent northeasterly winds, which are likely due to the negative Pacific Decadal Oscillation (PDO) during the period of study. Given the future scenarios on climate change and the threat it poses to reef islands, improving the health of the coral reefs is a must since the sediment that reefs provide dampens the erosive effects of sea-level rise and extreme-wave events.

*Corresponding Author: advcarrillo@gmail.com; +69612656020

INTRODUCTION

Atolls form through the upward growth of reef-building corals on top of a subsiding platform (Droxler and Jorry, 2021). Small, low-lying islands forming on the rims of these atolls are called atoll islands, or reef islands. These islands are mainly composed of loose or unconsolidated carbonate materials which are typically coral fragments, coralline or calcifying algae, mollusks, and foraminifera (Woodroffe and Biribo, 2011).

Small, reef islands with maximum elevations of less than 10 m and an area of less than 1 km^2 are more likely to experience shoreline change since these island types are more susceptible to marine inundation and are unstable due to their composition (Kumar *et al*., 2018). In the Western Pacific, atoll islands are projected to experience a disproportionately high risk in future island habitability due to the combined effects of sea-level rise, extreme El Niño events, increased storm frequency and intensity, and distance-source waves or swells (Duvat *et al*., 2021). Additionally, reef islands are also sensitive to anthropogenic activities such as land reclamation and construction of structures as indicated by studies in urban atolls (Ford, 2012; Yates *et al*., 2013).

The Philippines is chiefly composed of islands with an area of less than 1 km^2 or 100 ha, and these islands are mostly located in the southern parts of the archipelago. Takagi and Esteban (2016) found that tropical cyclones (TCs) have been moving in a more southward direction given the increase in TC passage within the 10°N-12°N latitudes between 1945 and 2013. TCs can generate extreme waves that can cause large geomorphic changes in the shoreline of reef islands (Duvat et al., 2020; Ford & Kench, 2016; Mann & Westphal, 2016; Tuck et al., 2021). Storms are in fact considered the primary influence on shoreline change in tropical islands (Rankey, 2011). The southward migration of TC activity along

*Corresponding Author: advcarrillo@gmail.com; +69612656020

with projected sea-level rise puts Philippine reef islands at risk to storm surges, flooding, and erosion. Unfortunately, very few studies focus on shoreline change in reef islands in the Philippines.

This study determines historical changes in the shoreline position of two reef islands in the West Philippine Sea with differing degrees of human activities and explores the possible causes of shoreline movement for each. The effects of anthropogenic structures are investigated in this study.

MATERIALS AND METHODS

Study sites

Located west of Palawan, Philippines is the Kalayaan Island Group (KIG). It is composed of several atoll systems and low-lying reef islands. These islands belong to the "Dangerous Grounds" which is an area underlain by continental crust that rifted from mainland Asia with the onset of spreading in the South China Sea (SCS) basin and has been undergoing post-rift thermal subsidence ever since (Hutchison & Vijayan, 2010).

Due to the geographic location and topography of the KIG, it is highly susceptible to climate change effects such as sea level rise. Relative sea-level rise in the West Philippine Sea has a rate of 4-6 mm/yr (Kahana *et al*., 2016) which is faster than the global average of 3.3 mm/yr (Guérou *et al*., 2023). Sea-level rise effects to reef islands in the region can be exacerbated by subsidence given that the islands are all sitting on atoll rims. Janer et al. (2023), estimated the subsidence rate of the West and East Pag-asa Reef atolls to be 0.3 to 1.3 mm/y. They argue that this subsidence has allowed the

*Corresponding Author: advcarrillo@gmail.com; +69612656020

maintenance of the atoll's morphology. The compounded effect of sea level rise and subsidence, however, makes these islands susceptible to coastal erosion.

Reef islands within the South China Sea basin have eroded over the past three decades (Liu et al., 2020). Due to the cost of high-resolution satellite imagery, the study used Landsat and Sentinel-2 satellite images which the authors used to estimate long-term (1989-2019) changes in island area. As of present, this is the only study of this type that has been done in the region.

Pag-asa Island and Lawak Island are two of several low-lying atoll reef islands belonging to the KIG (Figure 1). These islands are affected by seasonal wind, the Northeast Monsoon between November and February, and the Southwest Monsoon between June and October (PAGASA, n.d.). Archival data from the Joint Typhoon Warning Center (JTWC) show that the KIG is rarely hit by typhoons. In the last 20 years, most of the storms (TC) passed north of the region.

Pag-asa Island (Figure 1a) is located about 500 km from Puerto Princesa, Palawan, and is located atop the eastern rim of the West Pag-asa Reef Atoll. The perimeter of the West Pag-asa Atoll Lagoon is 27.2 km. The northern and southern coasts of Pag-asa Island face the open ocean, its eastern coast faces the channel between the West Pag-asa Atoll and the East Pag-asa Atoll, while its western coast faces the lagoon. A 1.3-km E-W-oriented runway, the Rancudo Airfield, cuts across the southern part of the island. Both ends of the runway extend onto the reef flat. A harbor was dredged on the northwest side of the island and its immediate surrounding area was reclaimed beginning in 2019. Tides around Pag-asa Island are mixed semi-diurnal with a mean tidal range of 0.87 meters

*Corresponding Author: advcarrillo@gmail.com; +69612656020

(NAMRIA, 2014). Villanoy & Mancebo (1998) infer that waves around the island propagate from the general direction of the Northeast monsoon and that circulation within the reef areas are driven mainly by wind or offshore currents impinging on the reefs.

Lawak Island (Figure 1b) is located 300 km from Puerto Princesa, Palawan and is 169.5 km W-SW of Pag-asa Island. The island is on the western rim of the Patag-Lawak Atoll. The perimeter of the lagoon of the Patag-Lawak Atoll is 48.2 km. The eastern coast of the island faces the lagoon while its western coast faces the open sea. Unlike Pag-asa Island, no man-made structures are jutting out of Lawak Island's coastline. Additionally, there are no previous studies focusing on Lawak Island.

Field survey

Field surveys were conducted on Pag-asa Island in April 2021, October 2021, February 2022, April 2022 and September 2022. to identify indicators of shoreline erosion and accretion. Such indicators include the displacement of structures relative to the shoreline, overwash deposits, exposed roots of beach vegetation, scarps, and lag deposits. Due to time constraints, only a short ocular survey was conducted on Lawak Island.

Beach Profiling

Beach profiling was only done in February 2022, April 2022 and September 2022. The Emery (1961) method (Figure 2) is used to measure the beach profiles and estimate the average beach slope of Pag-asa Island. Each measurement has an accuracy of up to 1

*Corresponding Author: advcarrillo@gmail.com; +69612656020

cm, however, it should be noted that the Emery method relies on the accuracy of each individual measurement since the readings are added together to obtain the beach profile. Beach profiles are corrected to the Mean Sea Level (MSL) by getting the difference between the recorded elevation and calculated difference between MSL and predicted tides. Predicted tides are calculated using the tide table and associated methods provided by the National Mapping and Resource Information Authority (NAMRIA, 2014). For Lawak Island, the beach slope is estimated from the collected photographs during the brief field survey around the island using the ImageJ application. For each image, an object with a known size is used as a reference for the calibration of the application before the actual measurement of the beach slope. The calculated and measured beach slope or slope of the beach face which starts from the storm berm to the elevation of the calculated MSL for Pag-asa and Lawak, respectively, are used to calculate uncertainty values due to tidal variation per the method proposed by Warnasuriya *et al*. (2018). Additionally, beach width is measured from the storm berm crest to the elevation of the MSL.

Shoreline Change Analysis

In this study, Google Earth images (Table 1 and 2) are georeferenced using ArcGIS 10.8.1 software. The high-water line (HWL) is used as an indicator of shoreline position to minimize the effect of tides on shoreline calculation. The HWL appears as the most landward dark line or the interface between wet and dry sand where wet sand appears darker. It represents the point on the beach reached by the high tide. If the HWL is not present, then it is assumed that the image is captured during the high tide. This method

*Corresponding Author: advcarrillo@gmail.com; +69612656020

is adopted since tide correction could not be accomplished since Google Earth images lack metadata. Manual digitization of Google Earth images for both islands is done using the ArcGIS 10.8.1 software. The HWL of Pag-asa Island is traced using the GPS unit during field surveys in February 2022 and April 2022. Additionally, area change for each island is also calculated from the resulting shoreline shapefiles by converting the shapefiles into polygons. The area of each polygon is calculated using the field calculator and the measured values are added or subtracted from previous values depending on whether the shoreline advanced or retreated.

The estimation of uncertainty associated with each shoreline position was based on Warnasuriya *et al*. (2018) which considers tidal variation, digitizing error, and geometric error. Since Google Earth images were georeferenced beforehand, geometric error was excluded from the calculation. The largest contributor to Total Uncertainty for the digitized shorelines of Pag-asa Island is tidal error. For shorelines traced using the handheld GPS device, the largest contributor is GPS error which is identified to be equal to ±3 m (Table 1).

Net Shoreline Movement (NSM), End Point Rate (EPR), and Linear Regression Rate (LRR) were then determined using the Digital Shoreline Analysis System (DSAS), an add-in to Esri ArcGIS desktop. Figure 3 shows the summary of the workflow used in the study. NSM measures the distance between the oldest and youngest shorelines in meters, EPR is the distance divided by the time between the oldest and youngest shoreline and LRR is determined through fitting a least-squares regression line to all points within the transect where each shoreline intersects (Himmelstoss *et al*., 2018).

*Corresponding Author: advcarrillo@gmail.com; +69612656020

Climate Data Analysis

In the absence of in-situ climate measurements within the KIG, estimations provided by satellite data were used (Table 3). Estimations were downloaded from the Copernicus Marine Data Store (https://data.marine.copernicus.eu/products) and the Copernicus Climate Data Store (https://cds.climate.copernicus.eu).

RESULTS

Field Surveys

Extensive erosion in the northern coast of Pag-asa Island and a relatively stable southern coast are observed during the ocular surveys. Man-made structures (Figures 4 and 5) along the coast that have been undercut (Figure 5f) or found seaward of the waterline (Figure 4b) are used as indicators of shoreline movement. Along the south beach, concentrations of gravel (Figure 5d) are associated with erosion that extended landward beyond the sheet piles of the runway on both ends (Figure 5f). Other indicators of erosion (Figures 5a-c,e) are also found around the island and are more prevalent on the northern coast compared to the southern coast.

The northern coast of Pag-asa Island is wide compared to its southern coast based on beach profile measurements. Mean beach slopes (Table 4) measured from the storm berm to the elevation of mean sea level (MSL), calculated from the NAMRIA tide table (NAMRIA, 2014), show that the northern coast is steep and has a less variable slope when compared to the southern coast.

*Corresponding Author: advcarrillo@gmail.com; +69612656020

Time Series of Changes in Shoreline Position

The calculated shoreline change statistics for Pag-asa Island are shown in Figure 6. Transects were grouped into six for ease of discussion. NSM, EPR, and LRR values follow a similar trend. Seventy-eight percent of the shoreline eroded while the remaining 22% accreted. Average shoreline statistics for each zone reveal that Zone C has the highest average erosion while Zone A is the only zone with observed accretion from 2005 to 2022.

Overall, NSM and LRR values for the northern coast of Pag-asa Island were -14.5 m and -0.88 ± 0.13 m/yr, respectively. While for the southern coast, NSM and LRR values were -3.7 m and -0.28 ± 0.15 m/yr, respectively. These numbers indicate that the island's northern coast eroded from 2005 to 2022 while the southern coast remained relatively stable. This is consistent with field observations. Figure 7 illustrates the pattern of cumulative area changes across different periods. Consistent with overall NSM and LRR values, the area of the northern coast declined, while the area of the southern coast was relatively stable.

Figure 8 shows the calculated shoreline change statistics for Lawak Island. Overall, NSM, EPR, and LRR values follow a similar trend. Shoreline change calculations indicate that the entire coast of Lawak Island was eroded by an average distance of -7.5 m (NSM) or -0.43 ± 0.22 m/yr (LRR). About 80% of the generated transects for this island were erosional while the remaining 20% were accretional. Lawak Island transects were divided into two zones based on the overall trend for ease of discussion. All segments of Zone B

*Corresponding Author: advcarrillo@gmail.com; +69612656020

were erosional while Zone A had alternating areas of erosion and accretion. Figure 8 also shows the average shoreline change statistics values for each zone.

Lawak Island experienced a net decrease in area over time from 2004 to 2021 (Figure 9). The western side lost 0.2 ha while the eastern side lost 0.5 ha. There were large fluctuations from 2009 to 2015 and smaller fluctuations in the following years. Between 2015 and 2019, area change in the eastern and western coasts of the island showed alternating trends. When the eastern coast was accreting, there was erosion in the western coast, and vice versa. Overall, the largest increase in the island's land area was between March 2011 to May 2012 at 1 ha, while the largest decrease at 1.4 ha was between October 2014 to December 2014.

DISCUSSION

Seasonal changes in shoreline position

Seasonal shifts in monsoon winds cause seasonal reversals in sediment flux and in turn seasonal shoreline changes (Kench & Brander, 2006). The East Asian Monsoon affects countries in Southeast Asia including the Philippines and consists of the East Asian summer monsoon (EASM) or the Southwest (SW) monsoon and the East Asian winter monsoon (EAWM) also known as the Northeast (NE) monsoon. Marchesiello et al. (2020) discussed that the NE monsoon, which is characterized by strong winds from the northeast, brings in heavy swells (>4m) due to high wind conditions with mean wind magnitude reaching 9 m/s and significant wave heights of 1- 2.5 m. Conversely, the SW monsoon, characterized by strong winds from the southwest, brings in 6 m/s winds and

*Corresponding Author: advcarrillo@gmail.com; +69612656020

weak waves about 0.8 m on average with tropical storms and typhoons causing significant wave heights to temporarily rise to around 4 m.

Wind data shows the seasonal shift of wind regimes (Figure 10) with the NE monsoon being more dominant than the SW monsoon. It also indicates that Pag-asa Island, relative to Lawak Island, experienced slightly stronger winds during the study period. Additionally, Google Earth images show that waves during the NE monsoon were generally better defined than waves during the SW monsoon.

Seasonal changes in wind direction were correlated with seasonal changes in shoreline position for both islands. However, Pag-asa Island (Figure 11) exhibited subdued seasonal changes in shoreline position, while larger shifts were exhibited by Lawak Island (Figure 12). Lawak Island becomes more elongated during the SW monsoon while during the NE monsoon, the northern and southern tips of the island become truncated.

Impact of structures.

The differences observed in the trends of shoreline change, especially for the seasonal changes, between Pag-asa Island and Lawak Island are attributed to the presence or absence of man-made structures along the shore. During the NE monsoon, the predominant direction of longshore drift along the eastern coast of Lawak Island is northward while along the western coast, it is southward (Figure 13a). During the SW monsoon, the wave patterns are similar but weaker based on waves breaking along the reef crest (Figure 13b). More waves are also observed to break along the western side of

*Corresponding Author: advcarrillo@gmail.com; +69612656020

the reef crest. The predominant direction of longshore drift remains the same, with minor changes in segments where it converges and diverges.

During the SW monsoon, more waves break along the western side of the island’s reef flat (Figure 14b). Wave patterns within the reef flat are similar to wave patterns during the NE monsoon, however, due to stronger waves coming from the western side of the island, longshore drift is modified. The largest change in shoreline position was along the northernmost portion of the island. This change is largely attributed to the construction of the port and harbor along the northwestern coast of the island in 2019.

Post-port and harbor construction, incoming waves from west of the island cause sediment along the outer portion of the harbor to drift towards the east (Figure 16), instead of following the east-to-west trend during the NE monsoon as discussed above. Longshore drift along the northeast portion of the coast remains the same.

There are no available Google Earth images taken during the SW monsoon post-port and harbor construction. However, based on the previous discussion, waves coming from the west would cause the predominant direction of longshore drift along the northwest coast of the island to reverse. The port and harbor would cause a decrease in the supply of sediment reaching the north by blocking the direction of longshore drift towards this portion of the island thereby causing flattening in the northern coast.

Before the construction of the runway and harbor, the circular shape of Pag-asa Island and the waves generated by shifting wind directions would likely produce reversing sediment drift directions around the island which would follow a pattern similar to Lawak Island (Figure 16). With the runway jutting out onto the reef flat on both ends, the sediment

*Corresponding Author: advcarrillo@gmail.com; +69612656020

exchange along the northern and southern coastlines was arrested. Furthermore, during the NE monsoon, sediment may get trapped on the northern side of the western end of the runway, and during the SW monsoon, sediment can be lost to the reef flat on the southern end of the eastern runway. These likely contributed to the eroding trend of the northern coastline.

The eastern side of Lawak Island faces the Patag-Lawak Atoll's lagoon while the western side of Pag-asa Island faces the West Pag-asa Atoll lagoon. The reef flats of both islands are more extensive on the north-northeastern side of each island, however, the reef flat of Pag-asa Island is four times the size of Lawak Island's reef flat. Lagoonward shores are expected to experience less wave energy but are more susceptible to sea-level rise given their lower elevation, however, this could be more variable due to other factors such as water depth, size of the lagoon, fetch (Woodroffe, 2008). Therefore, the lagoon's role in coastal protection could be attributed to the differing sizes and depths of the atoll lagoons to which each island belongs. Additionally, a more extensive reef flat area on the north-northeastern side of each island could lead to less energetic waves reaching each island in that direction and therefore less erosion.

Inter-annual changes caused by climate

Alternating warm and cold phases of El Niño-Southern Oscillation (ENSO) were experienced between 2000 and 2022 (Figure 17a) while cold phases of the Pacific Decadal Oscillation (PDO) dominated between 2000 and 2022 with warm phases occurring only between 2002 and 2005 as well as 2014 and 2016 (Figure 17b). The highest positive values for the multivariate ENSO index were recorded between 2014 and

*Corresponding Author: advcarrillo@gmail.com; +69612656020

2016 when it coincided with the Pacific Decadal Oscillation (PDO) warm phase. This warm phase of both the PDO and ENSO coincides with decreased typhoon activity in the region.

A major El Niño event was anticipated from 2014 to 2015, however, this failed to materialize and instead aided in the development of the 2015-2016 extreme El Niño event (Levine and McPhaden, 2016). El Niño events initially cause a weak East Asian Winter Monsoon (EAWM) with weaker waves and transport in the South China Sea basin, which is followed by a strong East Asian Summer Monsoon (EASM) that is further strengthened by a positive PDO phase (Marchesiello *et al*., 2020), as was the case between 2014 and 2016.

The 2015-2016 event was found to evolve as a Central Pacific El Niño event (Paek *et al*., 2017). Central Pacific El Niño events were identified to amplify north or northeasterly winds linked with the NE monsoon or EAWM (Kaboth-Bahr *et al*., 2021) however, this was not observed in the extracted wind data. Instead, this event was characterized by weaker SW monsoon winds coupled with slightly stronger NE monsoon winds as SW monsoon winds did not intensify until 2018.

The persistence of the negative phase of the PDO in the last two decades could have had a greater influence on the climate in the West Philippine Sea. Cold PDO phases (PDO-negative) and associated La Niña events are known to promote long-term strengthening of north and northeasterly winds and higher wave energy which in turn can encourage the southward transport of sediment in both Pag-asa and Lawak islands similar to that which occurred along the coast of central Vietnam (Marchesiello *et al*.,

*Corresponding Author: advcarrillo@gmail.com; +69612656020

2020). Stronger winds associated with the NE monsoon due to prolonged PDO cold phases and frequent La Niña events could have caused the northern coast of Pag-asa Island and the eastern coast of Lawak Island to be more prone to erosion.

Impact of extreme-wave events

The recorded significant wave height for both islands follows a similar pattern. However, the recorded wave heights for Lawak Island are lower by approximately 0.5 to 1 m (Figure 18). Twelve storm events, recorded to pass within a 500 km radius of Pag-asa and Lawak Islands, coincided with increased significant wave heights. All these storms formed in the Pacific and generally traversed the West Philippine Sea from east to west.

Significant wave height data shows that Super Typhoon Rai, locally named Super Typhoon Odette, caused the highest increase in significant wave height which was 1 m higher than other storms that have affected the area. In this section, the effects of super typhoon Odette will only be discussed for Pag-asa Island due to the absence of images for Lawak Island soon after the typhoon passed.

Figure 19a shows the track of super typhoon Odette as well as the average hourly wind speed and direction in Pag-asa Island during its passing. Average hourly wind data (Figure 19b) derived from satellite imagery show that wind speeds during the landfall of Typhoon Odette over Pag-asa Island on December 18, 2021, reached up to 23 m/s or 44.7 knots. Both the wind vector and wind rose diagrams (Figure 19c) show that wind direction was predominantly from the northeast, however, the strongest winds came from the west, south, and east.

*Corresponding Author: advcarrillo@gmail.com; +69612656020

Field observations indicate several meters of erosion on the northern coast based on the position of structures relative to the shoreline in the February 2022 survey compared to the April 2021 survey. Overwash deposits were found along the northern coast and the southwest coast beneath the western runway extension which suggests that storm surges may have impacted these areas during the typhoon.

In terms of area, Pag-asa Island lost about 0.5 ha of its total land area between March 2021 and February 2022. This loss is mostly along the northern coast since the southern coast remained relatively stable. The land area of the island continued to decline between February 2022 and April 2022, this time with both coasts receding.

Shoreline change statistics between May 2021 and February 2022 show that the northern coast eroded by an average distance of -2.6 m while the southern coast accreted by 8.4 m. Shoreline traces and shoreline change statistics (Figure 20) show that the landward migration of the shoreline is mostly in Zone C while seaward movement is mostly in Zones E and F.

Increased wave heights brought by Super Typhoon Odette transported sediment further inland leading to increased elevation of beach berms around the island. Unfortunately, beach profiles were not measured before Super Typhoon Odette, however, the presence of overwash deposits, identified during the field surveys, indicate an increase in beach elevation after the storm. This increase in elevation caused by extreme events such as Odette could be beneficial for the island in the long run, given the threat of sea-level rise and subsidence.

*Corresponding Author: advcarrillo@gmail.com; +69612656020

For Pag-asa Island, to replace the sediments that are now overwash deposits, a new supply of material from the reef flat is needed. Along the southern coast of Pag-asa Island, its relative stability could be indicative of pulses of recovery, since it has remained relatively stable despite the presence of multiple storms in the area throughout the years.

Sediment budget

The sediment supply for both islands was not quantified in this study, however, previous studies elsewhere suggest that sediment budget and the pathway of sediments can dictate whether the island will erode, accrete, or become stable overall. Most of the sediment in atoll islands come from the reef and reef flat environments (Perry *et al*., 2011) while some sediment might be allochthonous and directly transported by high-energy pulse events (Bonesso *et al*., 2022; Tuck *et al*., 2021).

The compounded effect of sea-level rise and subsidence make these islands susceptible to coastal erosion. Higher sea levels would result in larger waves (Storlazzi *et al*., 2015) which can surpass the height of the reef crests protecting the islands, causing erosion. Based on area growth rates, area growth speeds, and beach widths estimated by Liu *et al*. (2020), reef islands within the South China Sea basin have eroded over the past three decades. However, substantial sediment supply can dampen or offset the sea-level rise effects (Tuck *et al*., 2021). A healthy reef would ensure reef accretion which can continue the reef's efficacy in attenuating waves before they impact the islands (Villanoy and Mancebo, 2005). Therefore, keeping the surrounding reef healthy is important in maintaining the islands.

*Corresponding Author: advcarrillo@gmail.com; +69612656020

During storms, the recovery and the pace of recovery of reef islands are dictated by sediment fluxes around the reef rim and reef platform surface. Sediment can be made available to the beach because of the destruction of living corals during extreme-wave events allowing reef islands to maintain an equilibrium state (Duvat *et al*., 2017; Ford and Kench, 2014). Storm-built ridges at the reef-platform edge may influence hydrology on the reef platform and may dampen wave impact, as a natural process to reduce the effects of relative sea-level rise. Previous surveys in very similar environments have shown that most sediment transport and geomorphic changes may happen at the edges of the reef platform, as e.g. on Carbin Reef during Typhoon Haiyan (Reyes *et al*. 2015, Coral reefs: Brill *et al*. 2016). Projected increases in typhoon intensity may result in a larger sediment supply during each event, however, increased storm frequency would reduce coral recovery and growth, thereby reducing the sediment supply and exacerbating erosion (Tuck *et al*., 2021).

In the case of Pag-asa and Lawak islands, all the sediments, except those brought in for the construction of structures in Pag-asa Island, are from the reef and reef flat environments. In the satellite images, bright stripes from the northern and eastern portions of the reef crest of Pag-asa Island are sediments being transported by waves towards the inner reef flat and eventually onto the island (Figure 21). The dark areas are seagrass meadows that serve both as sediment traps and sources.

CONCLUSION

*Corresponding Author: advcarrillo@gmail.com; +69612656020

This study explored the different drivers of shoreline change and their effects on small, low-lying reef islands. Seasonal shifts in wind direction were found to cause shifts in longshore drift direction for both islands. Long-term trends in climate such as the interaction between PDO, ENSO, and the East Asian Monsoon were shown to contribute to long-term trends in shoreline movement while single storm events, such as Super Typhoon Odette, were shown to transport sediment onshore causing short-term erosion. Cold PDO phases and associated La Niña events are identified to have influenced southward transport of sediment in islands making the northern and eastern coasts of Pag-asa and Lawak Island, respectively, more prone to erosion. In Pag-asa Island, the runway jutting onto the reef flat modified sediment transport around the island and contributed to the erosion of the island. Due to the presence of structures, erosion in Pag-asa Island is exacerbated, while Lawak Island is more likely to recover despite experiencing a fluctuating changes in shoreline position given that the trend of area change for the island continues at an upward trend.

Given the results of this study, it is recommended that structures constructed on the islands and similar areas have none to minimal interference with the sediment drift around the islands. Additionally, sand mining within the vicinity of the islands should be avoided entirely. A healthy coral reef would also help in providing sediment for the islands and in attenuating incoming waves. Additionally, to further protect the reefs in the Kalayaan Island Group, it could be beneficial to establish multiple Marine Protected Areas in the region. Potential studies on shoreline change in reef islands within the West Philippine Sea would also benefit from an in-depth examination of the oceanography and

*Corresponding Author: advcarrillo@gmail.com; +69612656020

climatology of the region. Additionally, access to very high-resolution multi-spectral satellite imagery would improve the accuracy of future studies.

ACKNOWLEDGMENTS

This study was part of a project under Fernando P. Siringan which was funded by the national government and was supported by the University of the Philippines Diliman.

REFERENCES

BIRIBO N, WOODROFFE CD. 2013. Historical area and shoreline change of reef islands around Tarawa Atoll, Kiribati. Sustainability Science 8(3): 345–362.

BONESSO JL, BROWNE NK, MURLEY M, DEE S, CUTTLER MVW, PAUMARD V, BENSON D, O’LEARY M. 2022. Reef to island sediment connections within an inshore turbid reef island system of the eastern Indian Ocean. Sedimentary Geology 436(106177).

BRILL D, MAY SM, ENGEL M, REYES M, PINT A, OPITZ S, DIERICK M, GONZALO LA, ESSER S, BRUCKNER H. 2016. Typhoon Haiyan’s sedimentary record in coastal environments of the Philippines and its palaeotempestological implications. Natural Hazards Earth System Science 16: 2799-2822.

BROWN S, NICHOLLS RJ, BLOODWORTH A, BRAGG O, CLAUSS A, FIELD S, GIBBONS L, PLADAITE M, SZUPLEWSKI M, WATLING J, SHAREEF A, KHALEEL Z.

*Corresponding Author: advcarrillo@gmail.com; +69612656020

2023. Pathways to sustain atolls under rising sea levels through land claim and island raising. Environmental Research: Climate 2(1).

CHEN W, FENG J, WU R. 2013. Roles of ENSO and PDO in the Link of the East Asian Winter Monsoon to the following Summer Monsoon. Journal of Climate 26(2): 622–635.

DROXLER AW, JORRY SJ. 2021. The Origin of Modern Atolls: Challenging Darwin's Deeply Ingrained Theory. Annual Review of Marine Science 13: 537–573.

DUVAT VKE, SALVAT B, SALMON C. 2017. Drivers of shoreline change in atoll reef islands of the Tuamotu Archipelago, French Polynesia. Global and Planetary Change 158: 134–154.

DUVAT VKE, PILLET V, TEROROTUA H, LAURENT V. 2020. Contribution of moderate climate events to atoll island building (Fakarava Atoll, French Polynesia). Geomorphology 354.

DUVAT VKE, MAGNAN AK, PERRY CT, SPENCER T, BELL JD, WABNITZ CC, WEBB AP, WHITE I, MCINNES KL, GATTUSO JP, GRAHAM NAJ, NUNN PD, COZANNET GL. 2021. Risks to future atoll habitability from climate-driven environmental changes. Wiley Interdisciplinary Reviews Climate Change 12(3): 1–28.

EMERY KO. 1961. A Simple Method of Measuring Beach Profiles. Limnology and Oceanography 6(1): 90–93.

FORD MR. 2012. Shoreline changes on an urban atoll in the central Pacific Ocean: Majuro atoll, Marshall Islands. Journal of Coastal Research 28(1): 11–12.

*Corresponding Author: advcarrillo@gmail.com; +69612656020

FORD MR, KENCH PS. 2014. Formation and adjustment of typhoon-impacted reef islands interpreted from remote imagery: Nadikdik Atoll, Marshall Islands. Geomorphology 214: 216–222.

FORD MR, KENCH PS. 2016. Spatiotemporal variability of typhoon impacts and relaxation intervals on Jaluit Atoll, Marshall Islands. Geology 44(2): 159-162.

GUÉROU A, MEYSSIGNAC B, PRANDI P, ABLAIN M, RIBES A, BIGNALET-CAZALET F. 2023. Current observed global mean sea-level rise and acceleration estimated from satellite altimetry and the associated measurement uncertainty. Ocean Science 19: 431–451.

HAU N, SANO M, NAKATSUKA T, CHEN S, CHEN, I. 2023. The modulation of Pacific Decadal Oscillation on ENSO-East Asian summer monsoon relationship over the past half-millennium. Science of the Total Environment 857(2).

HIMMELSTOSS E, HENDERSON RE, KRATZMANN MG, FARRIS AS. 2018. Digital Shoreline Analysis System (DSAS) version 5.0 user guide. U.S. Geological Survey Open-File Report 2018–1179.

HUTCHISON CS, VIJAYAN VR. 2010. What are the Spratly Islands? Journal of Asian Earth Sciences 39(5): 371-385.

JANER DFS, GABUYO MRP, CARRILLO ADV, CO PEY, DEL ROSARIO ALB, MORATA MJS, DAYAO JB, DE CHAVEZ MM, BRINGAS DAB, VILLANOY CL, SIRINGAN FPS. 2023. Development of Pag-asa Reefs, West Philippine Sea: Role of Relative Sea Level Change and Wave Exposure. Philippine Journal of Science 152(1): 291-306.

*Corresponding Author: advcarrillo@gmail.com; +69612656020

KABOTH-BAHR S, BAHR A, ZEEDEN C, YAMOAH KA, LONE MA, CHUANG C, LOWENMARK L, WEI K. 2021. A tale of shifting relations: East Asian summer and winter monsoon variability during the Holocene. Scientific Reports 11.

KAHANA R, ABDON R, DARON J, SCANNELL C. 2016. Projections of mean sea level change for the Philippines. Met Office. Retrieved from https://www.researchgate.net/publication/320800587_Projections_of_mean_sea_level_change_for_the_Philippines.

KENCH PS, BRANDER RW. 2006. Response of reef island shorelines to seasonal climate oscillations: South Maalhosmadulu atoll, Maldives. Journal of Geophysical Research: Earth Surface 111(1): 1-12.

KUMAR L, ELIOT I, NUNN P, STUL T, MCLEAN R. 2018. An indicative index of physical susceptibility of small islands to coastal erosion induced by climate change: An application to the Pacific Islands. Geomatics, Natural Hazards and Risk 9(1): 691–702.

LEVINE AFZ, MCPHADEN MJ. 2016. How the July 2014 easterly wind burst gave the 2015-2016 El Niño a head start. Geophysical Research Letters 43(12): 6503–6510.

LIU J, HUANG R, YU K, ZOU B. 2020. How lime-sand islands in the South China Sea have responded to global warming over the last 30 years: Evidence from satellite remote sensing images. Geomorphology 371: 1–12.

MAGNAN AK, DUVAT VKE. 2020. Towards adaptation pathways for atoll islands: Insights from the Maldives. Regional Environmental Change 20.

*Corresponding Author: advcarrillo@gmail.com; +69612656020

MANN T, WESTPHAL H. 2016. Multi-decadal shoreline changes on Taku Atoll, Papua New Guinea: Observational evidence of early reef island recovery after the impact of storm waves. Geomorphology 257: 75-84.

MARCHESIELLO P, KESTENARE E, ALMAR R, BOUCHAREL J, NGUYEN N. 2020. Longshore drift produced by climate-modulated monsoons and typhoons in the South China Sea. Journal of Marine Systems 211.

NATIONAL MAPPING AND RESOURCE INFORMATION AUTHORITY. 2014. Tides and Currents Tables.

PAEK H, YU J, QIAN C. 2017. Why were the 2015/2016 and 1997/1998 extreme El Niños different?. Geophysical Research Letters 44(4): 1848–1856.

Philippine Atmospheric Geophysical and Astronomical Services Administration (PAGASA). (n.d.). Climate of the Philippines. Retrieved from https://kidlat.pagasa.dost.gov.ph/index.php/climate-of-the-philippines on 10 August 2023.

PERRY CT, KENCH PS, SMITHERS SG, RIEGL B, YAMANO H, O'LEARY MJ. 2011. Implications of reef ecosystem change for the stability and maintenance of coral reef islands. Global Change Biology 17: 3679–3696.

RANKEY EC. 2011. Nature and stability of atoll island shorelines: Gilbert Island chain, Kiribati, equatorial Pacific. Sedimentology 58: 1831–1859.

REYES M, ENGEL M, MAY SM. 2015. Life and death after super typhoon Haiyan. Coral Reefs 34:419.

*Corresponding Author: advcarrillo@gmail.com; +69612656020

STORLAZZI, C. D., ELIAS, E. P. L., and BERKOWITZ, P. 2015. Many Atolls May be Uninhabitable Within Decades Due to Climate Change. Scientific Reports 5: 1–9.

TAKAGI H, ESTEBAN M. 2016. Statistics of tropical cyclone landfalls in the Philippines: unusual characteristics of 2013 Typhoon Haiyan. Natural Hazards 80(1): 211–222.

TUCK ME, FORD MR, KENCH PS, MASSELINK G. 2021. Sediment supply dampens the erosive effects of sea-level rise on reef islands. Scientific Reports 11.

VILLANOY C, MANCEBO F. 1998. Sea Level and Shallow Water Current Variability in Pagasa Island, Philippines. Science Diliman 10(2): 47–54.

WANG L, CHEN W, HUANG R. 2008. Interdecadal modulation of PDO on the impact of ENSO on the East Asian winter monsoon. Geophysical Research Letters 35.

WARNASURIYA TWS, GUNAALAN K, GUNASEKARA S. 2018. Google Earth: A New Resource for Shoreline Change Estimation – Case Study from Jaffna Peninsula, Sri Lanka. Marine Geodesy 41(6): 546–580.

WOODROFFE, C. D. 2008. Reef-island topography and the vulnerability of atolls to sea-level rise. Global and Planetary Change, 62(1–2): 77–96.

WOODROFFE CD, BIRIBO N. 2011. Atolls. In: Encyclopedia of Modern Coral Reefs: structure, form and process. Netherlands: Springer: p. 55–71.

YATES ML, LE COZANNET G, GARCIN M, SALAI E, WALKER P. 2013. Multidecadal atoll shoreline change on Manihi and Manuae, French Polynesia, Journal of Coastal Research 29(4): 870–882.

*Corresponding Author: advcarrillo@gmail.com; +69612656020

Table 1. Data source with respective dates of acquisition and calculated uncertainty values per shoreline for Pag-asa Island. Spatial resolution is retrieved from the Maxar website (https://discover.maxar.com), data source of Google Earth Pro.

Date of acquisition	**Spatial Resolution (m)**	**Digitizing Error (m)**		**Tidal Error (m)**		**GPS Error (m)**	**Total Uncertainty (m)**	
		North	South	North	South		North	South
April 22, 2005	0.64	0.56	0.40	1.83	1.75		2.39	2.15
February 25, 2007	0.65	1.07	1.02	1.83	1.75		2.90	2.77
January 8, 2014		1.01	0.82	1.83	1.75		2.84	2.57
March 4, 2014	0.60	0.95	0.58	1.83	1.75		2.78	2.33
April 28, 2015	0.56	1.58	0.75	1.83	1.75		3.41	2.50
August 17, 2015	0.52	0.80	0.61	1.83	1.75		2.63	2.36
March 6, 2016	0.36	1.17	0.53	1.83	1.75		3.00	2.28
November 29, 2016	0.41	0.84	0.52	1.83	1.75		2.67	2.27

*Corresponding Author: advcarrillo@gmail.com; +69612656020

February 16, 2017	0.41	0.95	0.68	1.83	1.75		2.78	2.42
September 17, 2017	0.34	1.33	0.94	1.83	1.75		3.16	2.69
February 24, 2018	0.5	0.59	0.65	1.83	1.75		2.42	2.40
August 12, 2018		0.78	0.71	1.83	1.75		2.61	2.46
April 23, 2019	0.33	0.57	0.51	1.83	1.75		2.40	2.26
March 27, 2021	0.35	0.66	1.06	1.83	1.75		2.50	2.81
May 16, 2021	0.32	2.04	0.92	1.83	1.75		3.87	2.67
February 24, 2022				1.83	1.75	3.00	4.83	4.75
April 9, 2022					1.75	3.00		4.75
April 11, 2022				1.83		3.00	4.83	

*Corresponding Author: advcarrillo@gmail.com; +69612656020

Table 2. Data source with respective dates of acquisition and calculated uncertainty values per shoreline for Lawak Island. Spatial resolution is retrieved from the Maxar website (https://discover.maxar.com), data source of Google Earth Pro.

Date of acquisition	Spatial Resolution (m)	Digitizing Error (m)	Tidal Error (m)	Total Uncertainty
March 4, 2004	0.62	0.52	4.12	4.63
June 11, 2009	0.49	0.63	4.12	4.75
May 25, 2010	0.50	0.46	4.12	4.58
March 18, 2011	0.48	0.59	4.12	4.71
May 29, 2012	0.58	0.62	4.12	4.74
April 5, 2014		0.42	4.12	4.54
October 15, 2014	0.37	0.54	4.12	4.66
December 27, 2014	0.46	1.44	4.12	5.56
February 19, 2015	0.54	0.55	4.12	4.67
February 7, 2017	0.52	0.71	4.12	4.83
May 29, 2017	0.51	0.73	4.12	4.85
November 15, 2017	0.44	0.81	4.12	4.93

*Corresponding Author: advcarrillo@gmail.com; +69612656020

February 20, 2018	0.33	0.54	4.12	4.66
December 7, 2018		0.84	4.12	4.96
March 19, 2019	0.45	0.61	4.12	4.73
February 04, 2021		0.75	4.12	4.87

*Corresponding Author: advcarrillo@gmail.com; +69612656020

Table 3. Summary of climate datasets used for this study.

Parameter	Dataset Name	Spatial Resolution	Temporal Resolution	Source
Sea level anomaly	Sea level gridded data	0.25° × 0.25°	Daily	Copernicus Climate Change Service, Climate Data Store
Significant wave height	ERA5 Global Atmospheric Reanalysis	0.5° × 0.5°	Hourly	Copernicus Climate Change Service, Climate Data Store
Wind speed and direction (2000-2019)	Global Ocean Wind L4 Near Real Time 6 hourly observations	0.25° × 0.25°	Hourly	Copernicus Marine Service
Wind speed and direction (2020-2022)	Hourly Global Ocean Sea Surface Wind and Stress from Scatterometer and Model	0.25° × 0.25°	Hourly	Copernicus Marine Service
Tropical cyclones	Best track archive			Joint Typhoon Warning Center (JTWC)
PDO phases	Pacific Decadal Oscillation (PDO) index		Bi-monthly	National Centers for Environmental Information, National Oceanic and Atmospheric Administration

*Corresponding Author: advcarrillo@gmail.com; +69612656020

ENSO phases	Multivariate ENSO Index		Monthly	National Centers for Environmental Information, National Oceanic and Atmospheric Administration

*Corresponding Author: advcarrillo@gmail.com; +69612656020

Table 4. Beach slope measurements per coast per survey in Pag-asa Island. The values presented are the mean beach slopes calculated from the beach profiling stations for February 2022 and April 2022 surveys done in Pag-asa Island.

Month	North	South
February	23.9°	28.7°
April	23.7°	22.3°
September	23.7°	20.7°

*Corresponding Author: advcarrillo@gmail.com; +69612656020

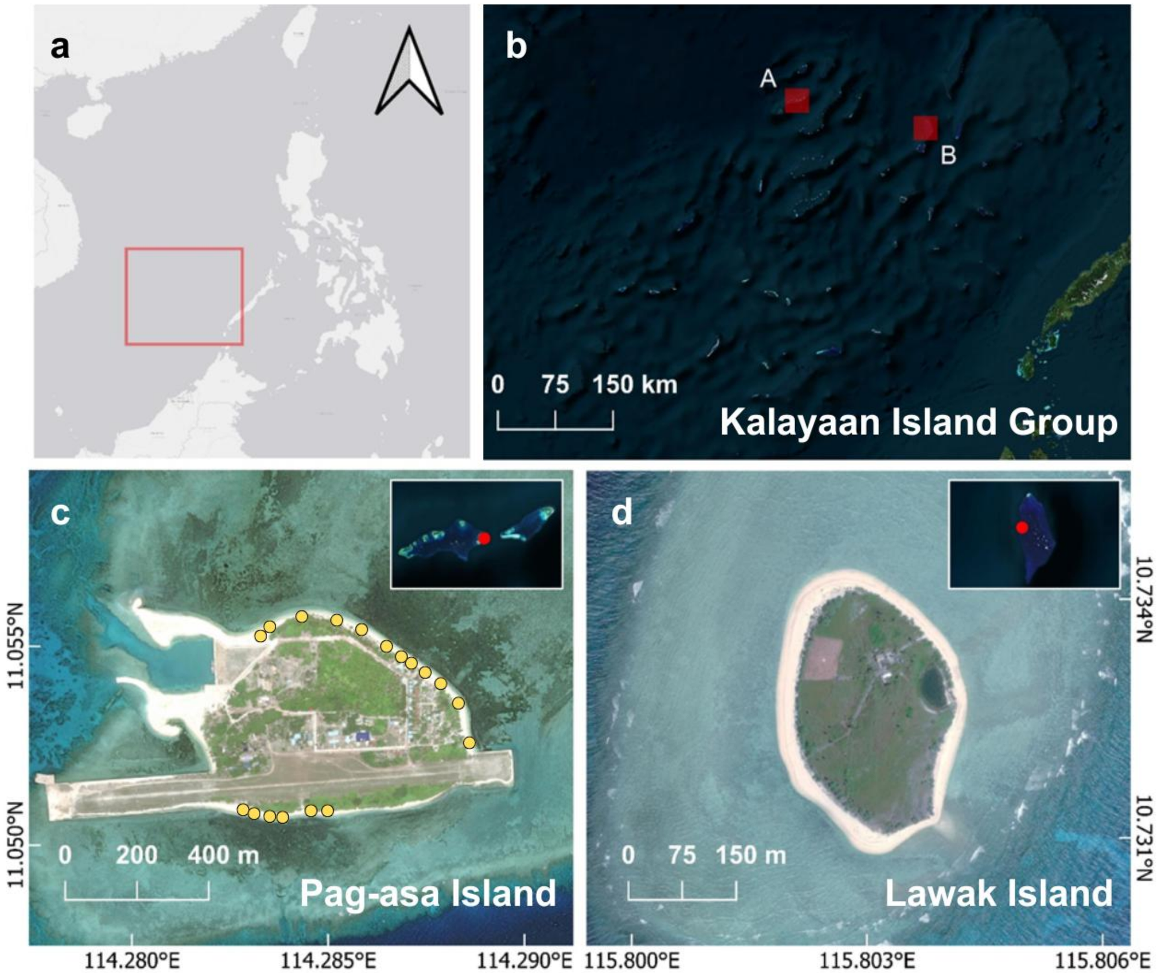

Figure 1. Location map of the (a) Kalayaan Island Group, (b) study sites and islands (c) Pag-asa and (d) Lawak. The yellow dots in panel c are the locations where beach slopes are measured. (Basemap source: Bing VirtualEarth, Map data © 2023 Microsoft)

*Corresponding Author: advcarrillo@gmail.com; +69612656020

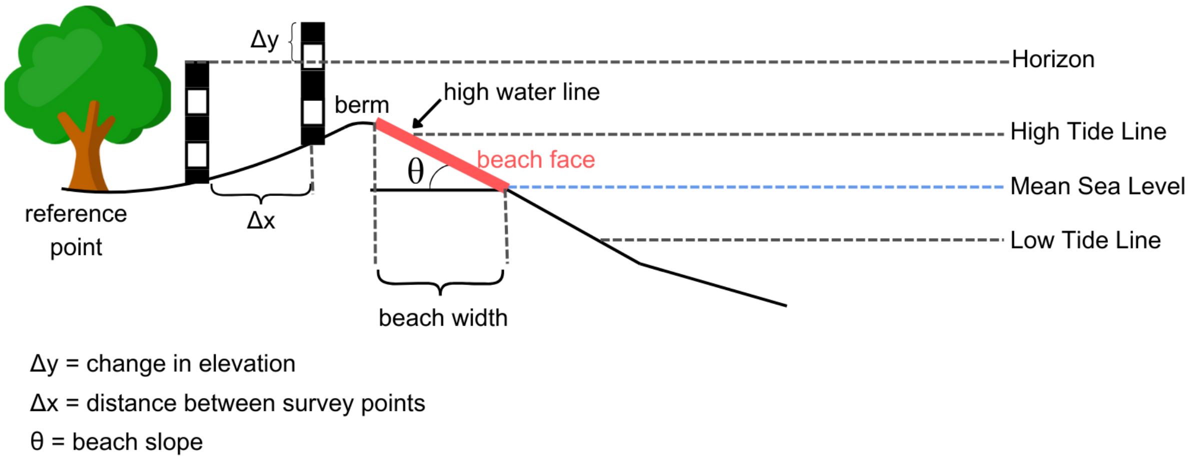

Figure 2. Illustration of the Emery Rod method and measurement of beach slope and beach width.

*Corresponding Author: advcarrillo@gmail.com; +69612656020

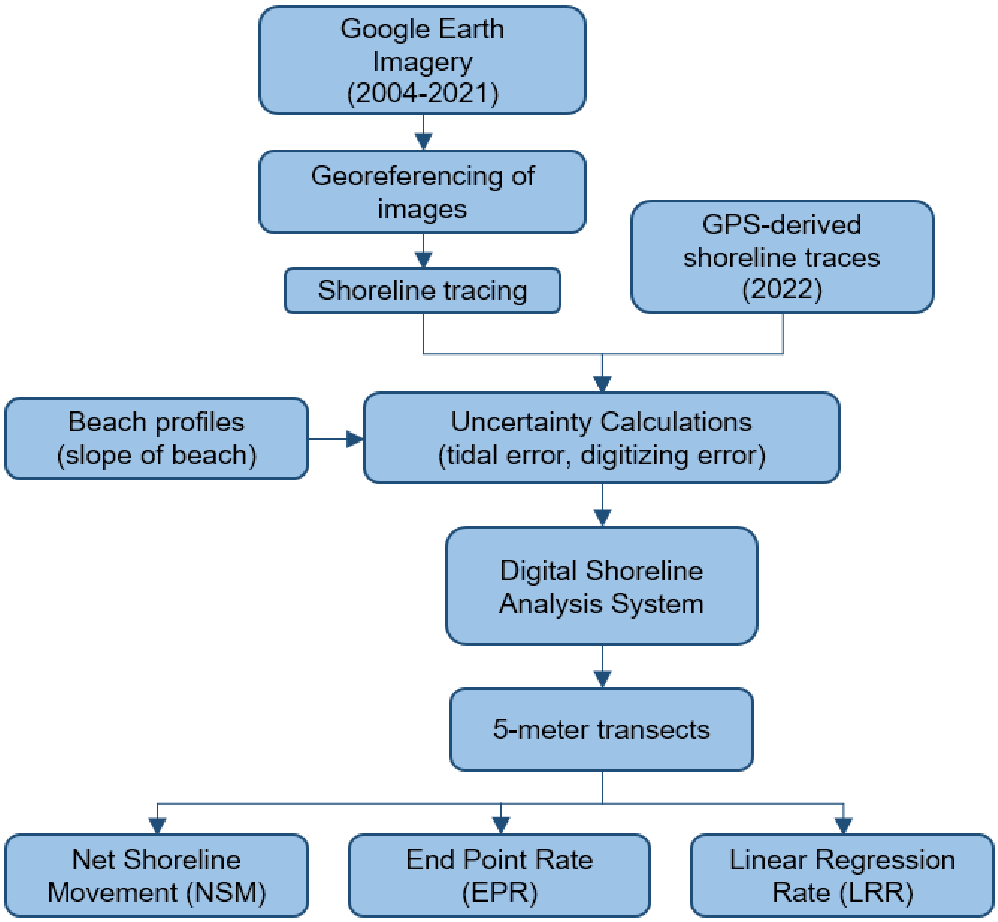

Figure 3. Summary of the workflow used for shoreline change analysis.

*Corresponding Author: advcarrillo@gmail.com; +69612656020

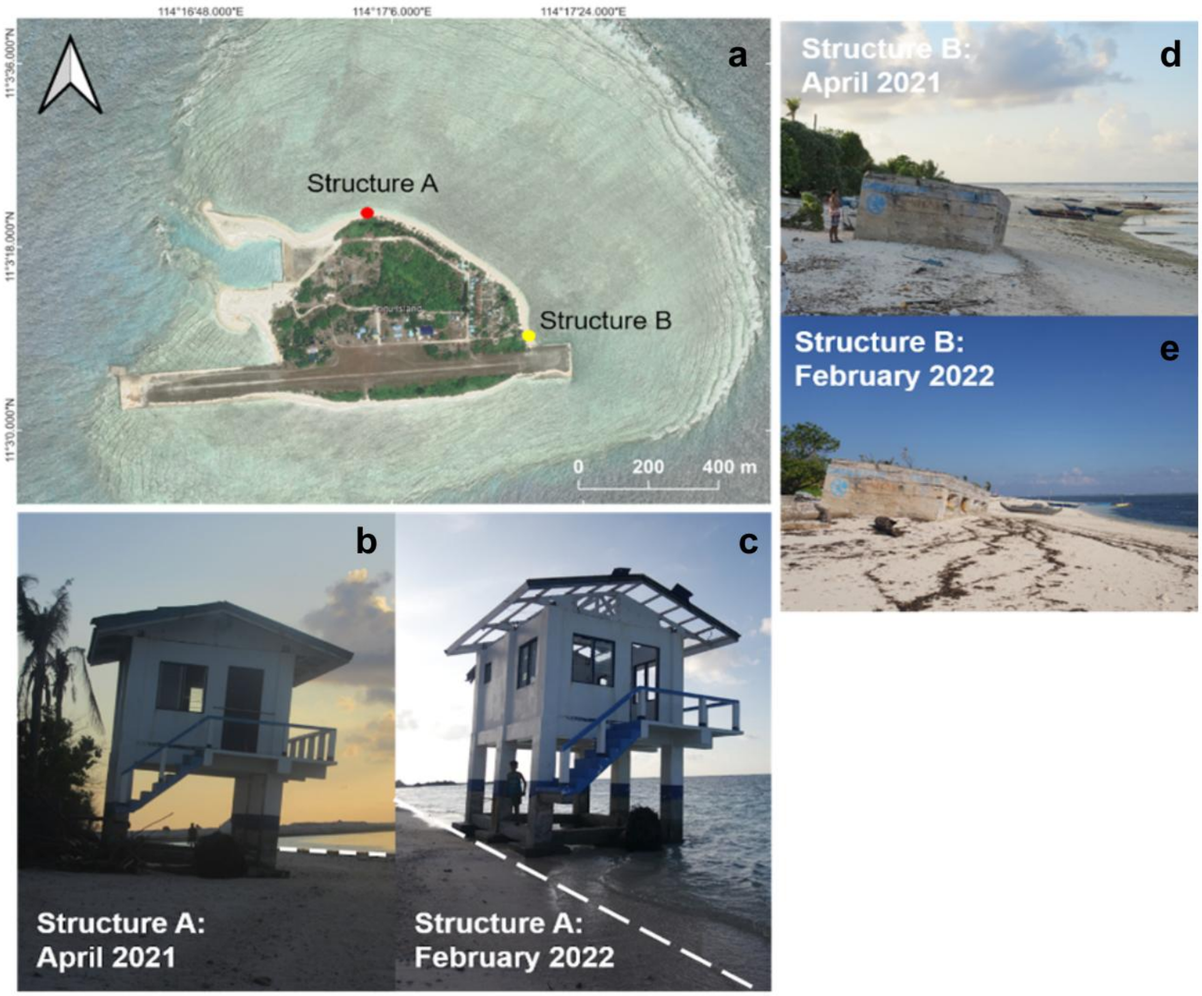

Figure 4. Man-made structures (a) used as reference for relative shoreline movement. Photos were taken in April 2021 (b, d) and February 2022 (c, e). The broken white lines show the waterline during the time the images were taken.

*Corresponding Author: advcarrillo@gmail.com; +69612656020

Figure 5. Various indicators of erosion such as (a) exposed plant roots, (b) uprooted trees, (c) beach scarps, (d) concentration of gravel sized sediments, (e) washed up deposits of plant debris, and (f) steel pilings showing where the shoreline should have been for Pag-asa Island.

*Corresponding Author: advcarrillo@gmail.com; +69612656020

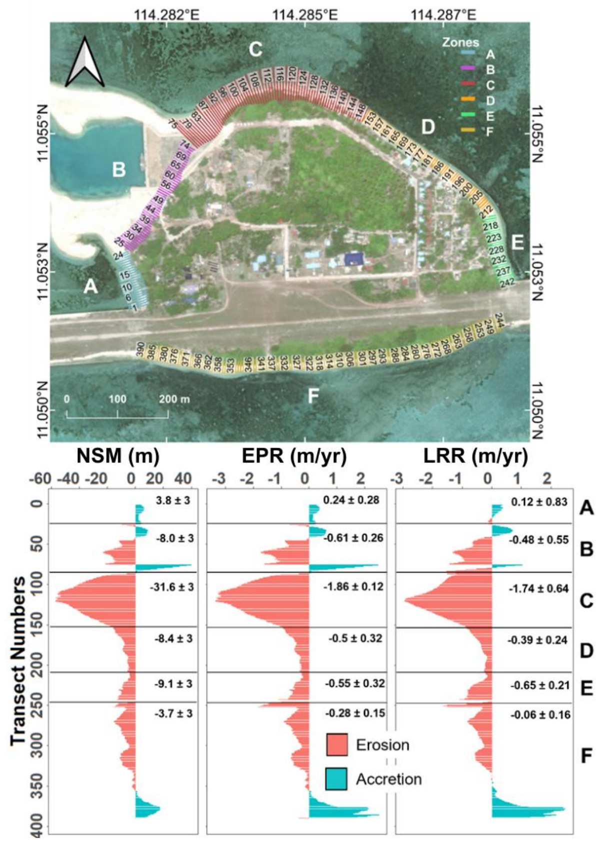

Figure 6. Transect locations and shoreline change statistics calculations in meters for Pag-asa Island. Net Shoreline Movement (NSM), End Point Rate (EPR), and Linear Regression Rate (LRR) were then calculated using the Digital Shoreline Analysis System (DSAS), an add-in to Esri ArcGIS desktop. NSM measures the distance between the oldest and youngest shorelines for each transect in meters, EPR is the distance between the oldest and youngest shoreline divided by the time elapsed between the two shorelines and LRR is determined through fitting a least-squares regression line to all shoreline points for a transect (Himmelstoss et al., 2018). The numbers on the right side of each panel are averages in meters. (Basemap source: Bing VirtualEarth, Map data © 2023 Microsoft)

*Corresponding Author: advcarrillo@gmail.com; +69612656020

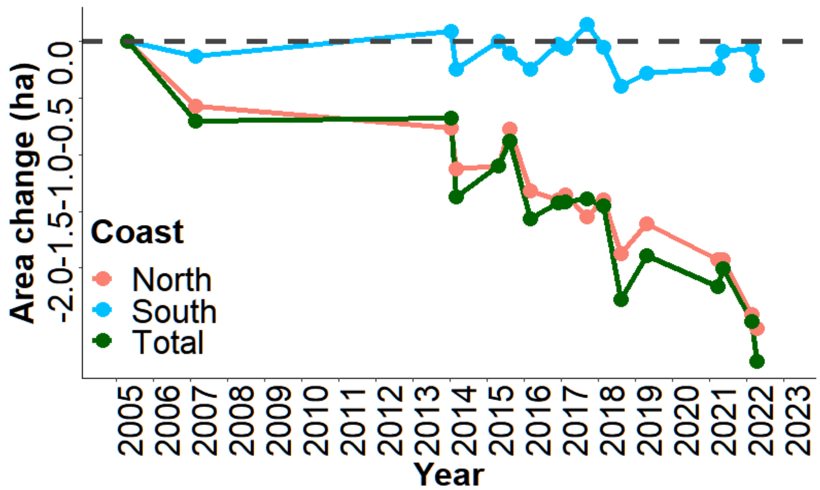

Figure 7. Area change calculations for Pag-asa Island. The green line is the total area change, the pink line is for the southern coast while the blue line is for the southern coast.

*Corresponding Author: advcarrillo@gmail.com; +69612656020

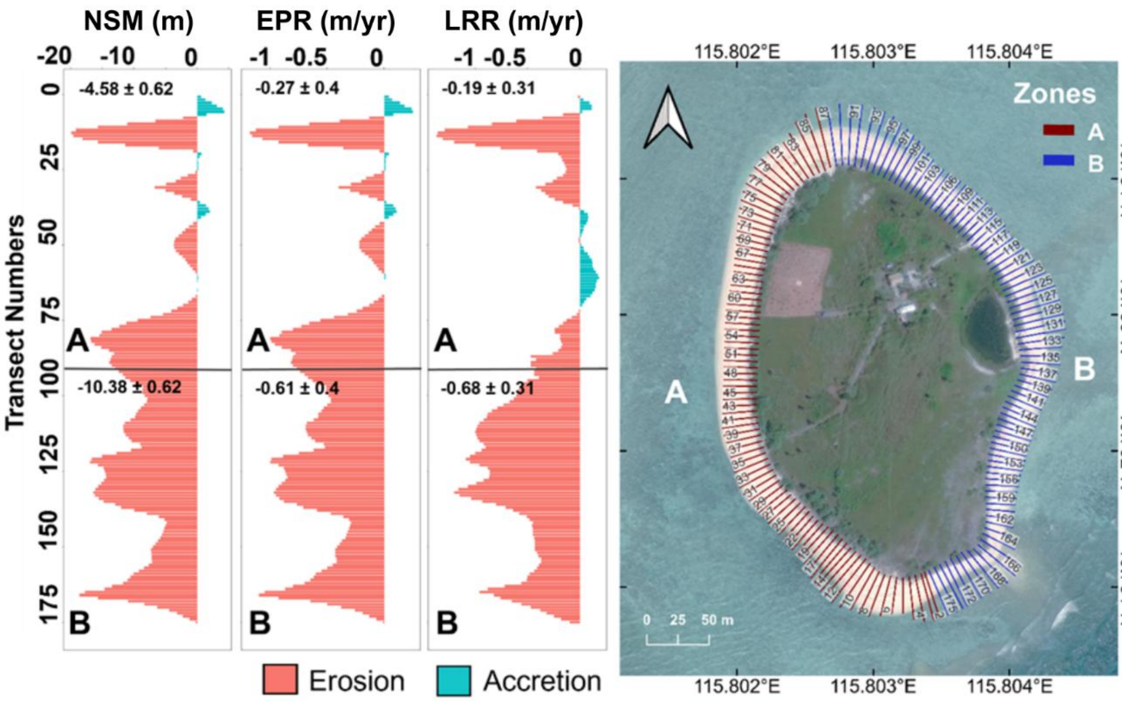

Figure 8. Transect locations and calculated shoreline change statistics in meters for Lawak Island. T Net Shoreline Movement (NSM), End Point Rate (EPR), and Linear Regression Rate (LRR) were then calculated using the Digital Shoreline Analysis System (DSAS), an add-in to Esri ArcGIS desktop. The numbers on the right side of each panel are averages in meters. (Basemap source: Bing VirtualEarth, Map data © 2023 Microsoft)

*Corresponding Author: advcarrillo@gmail.com; +69612656020

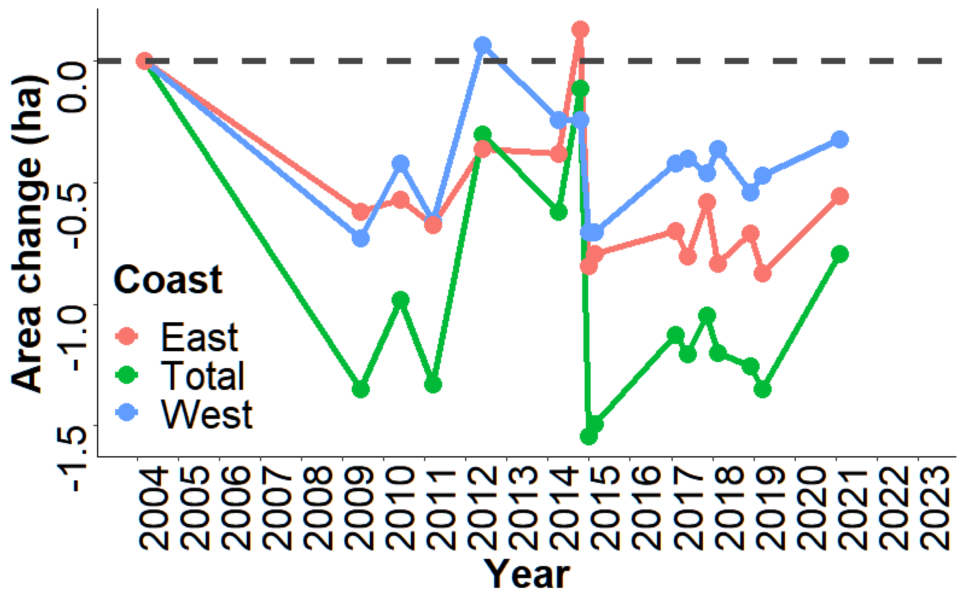

Figure 9. Area change calculations for Lawak Island.

*Corresponding Author: advcarrillo@gmail.com; +69612656020

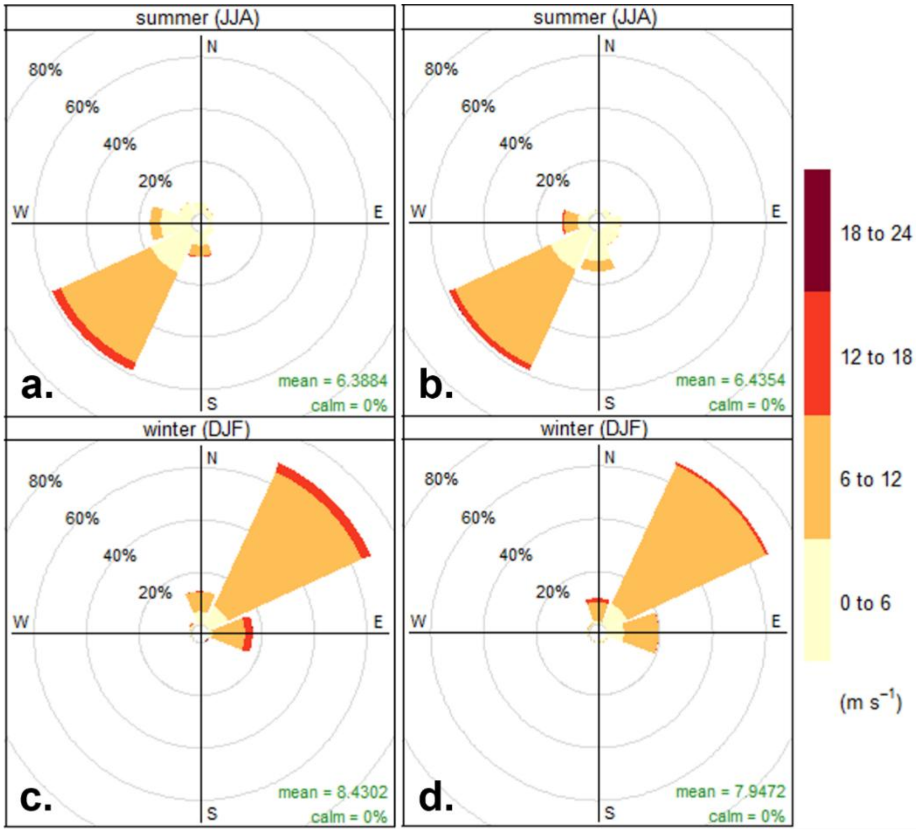

Figure 10. The wind rose diagrams for Pag-asa Island (a,c) and Lawak Island (b,d) constructed from hourly wind data between 2000 and 2022 (Data Source: Copernicus Marine Service).

*Corresponding Author: advcarrillo@gmail.com; +69612656020

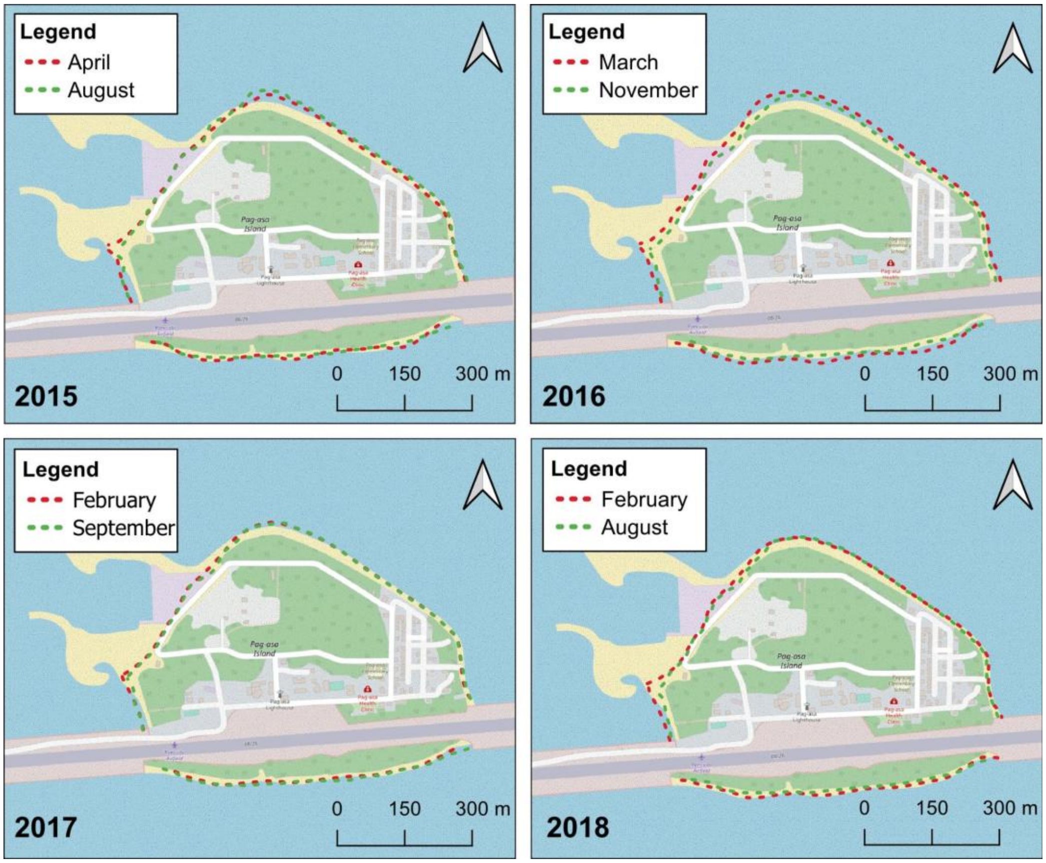

Figure 11. Seasonal shoreline position changes for Pag-asa Island. The red broken lines show shoreline traces during the NE monsoon while the green broken lines show shoreline traces during the SW monsoon (Basemap source: modified from OpenStreetMap).

*Corresponding Author: advcarrillo@gmail.com; +69612656020

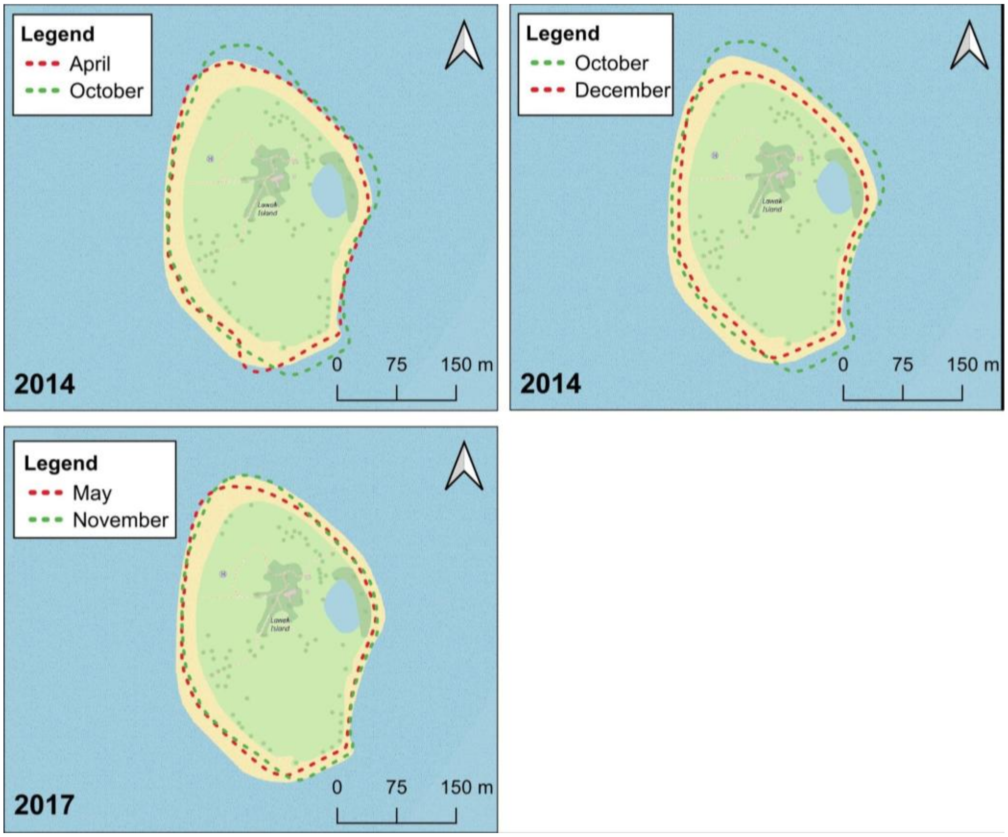

Figure 12. Seasonal changes in the shoreline position of Lawak Island. (Basemap source: OpenStreetMap)

*Corresponding Author: advcarrillo@gmail.com; +69612656020

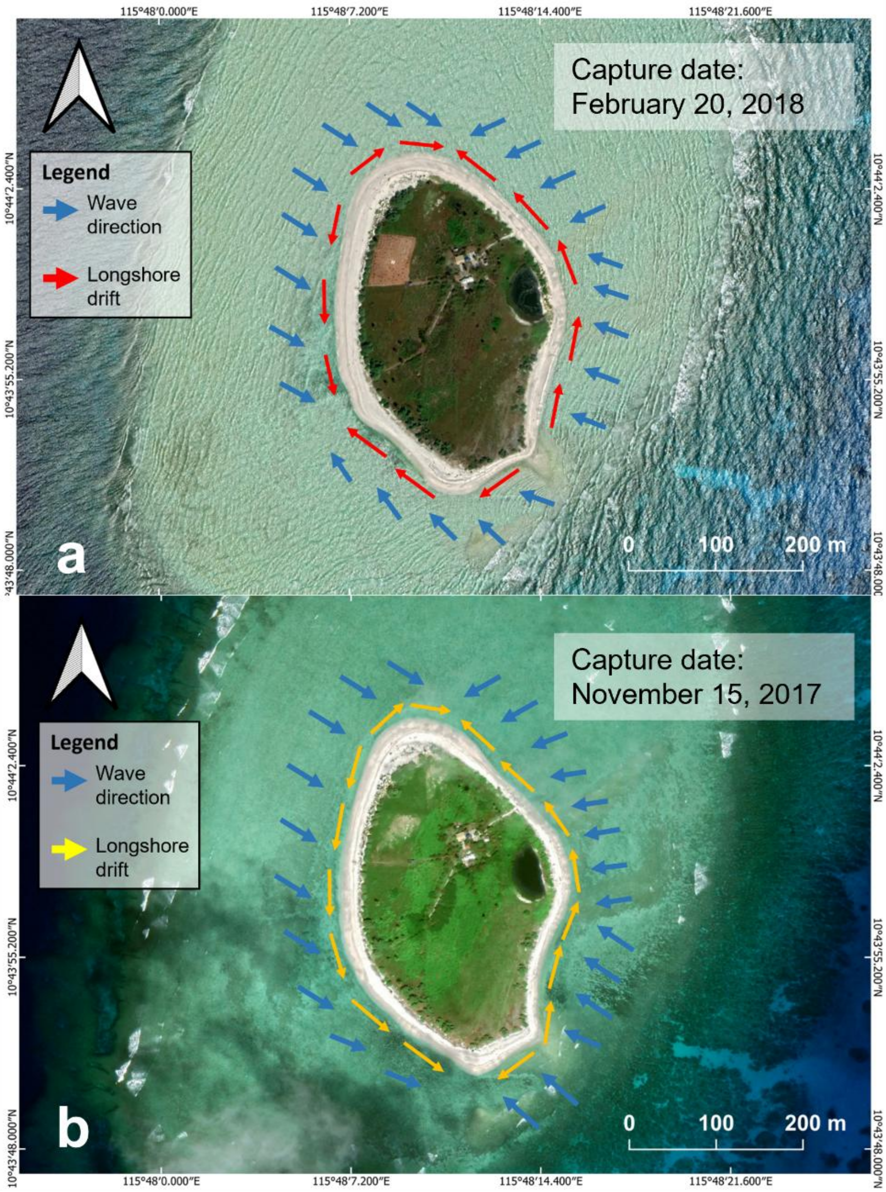

Figure 13. Wave refraction patterns and longshore drift along the coast of Lawak Island during the (a) Northeast Monsoon and (b) Southwest Monsoon. (Basemap source: Google Earth Pro, Map data © 2023 Maxar Technologies)

*Corresponding Author: advcarrillo@gmail.com; +69612656020

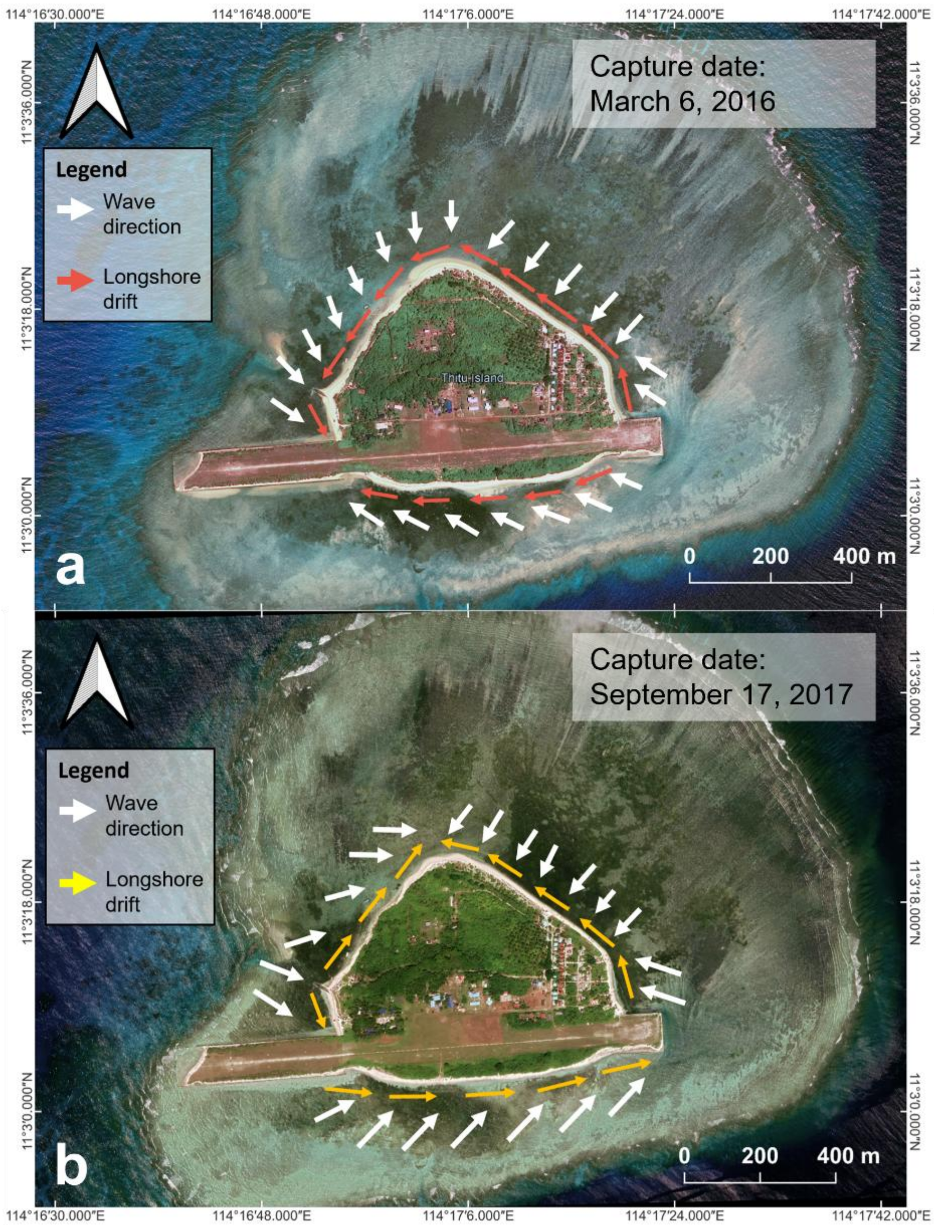

Figure 14. Wave refraction and longshore drift patterns along the coast of Pag-asa Island before port and harbor construction. The images were taken during the (a) Northeast Monsoon and (b) Southwest Monsoon. (Basemap source: Google Earth Pro, Map data © 2023 Maxar Technologies).

*Corresponding Author: advcarrillo@gmail.com; +69612656020

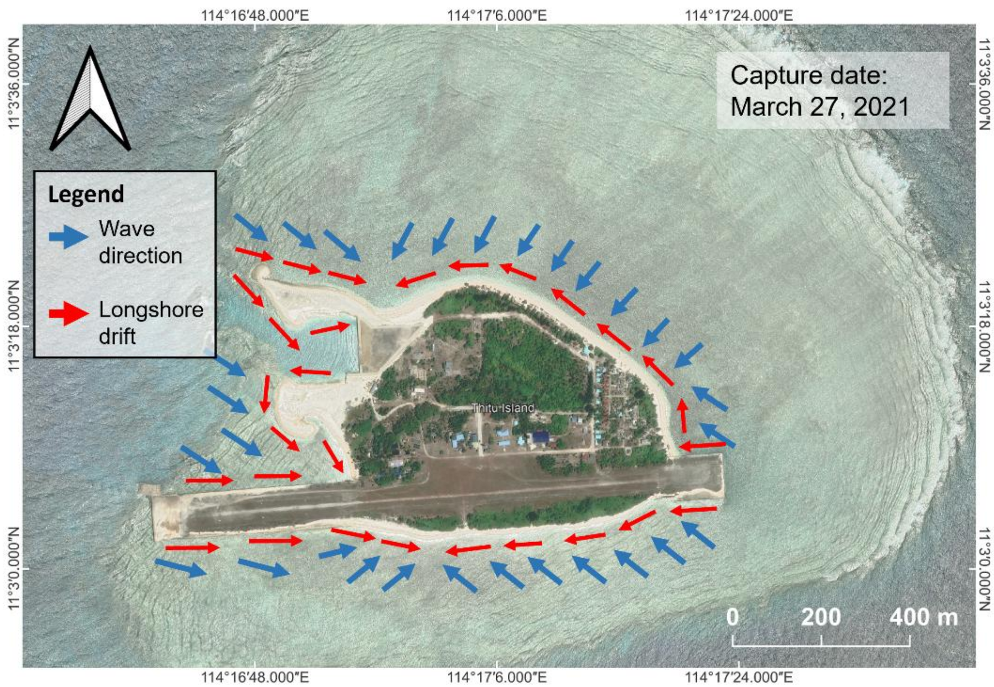

Figure 15. Wave refraction patterns and longshore drift along the coast of Pag-asa Island after port and harbor construction. The image was taken during the Northeast Monsoon. (Basemap source: Google Earth Pro, Map data © 2023 Maxar Technologies)

*Corresponding Author: advcarrillo@gmail.com; +69612656020

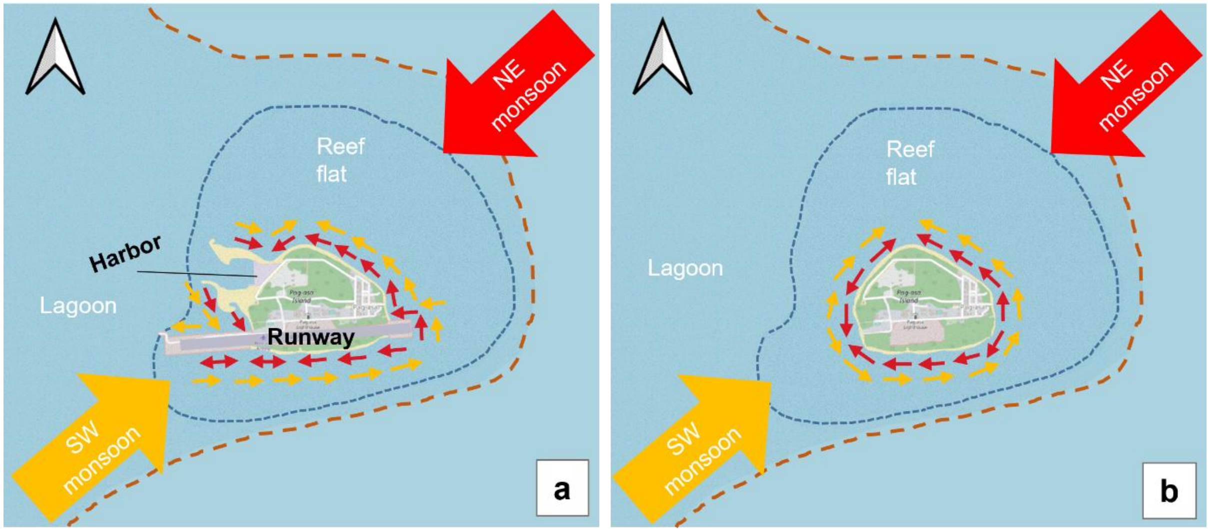

Figure 16. Longshore drift around Pag-asa Island during different seasons with (a) and (b) without structures. The broken lines represent the boundaries between the reef flat and the lagoon (blue) and the lagoon and the open ocean (orange). The red arrows show longshore drift direction during the Northeast Monsoon while the orange arrows show longshore drift direction during the Southwest Monsoon (Basemap source: modified from OpenStreetMap).

*Corresponding Author: advcarrillo@gmail.com; +69612656020

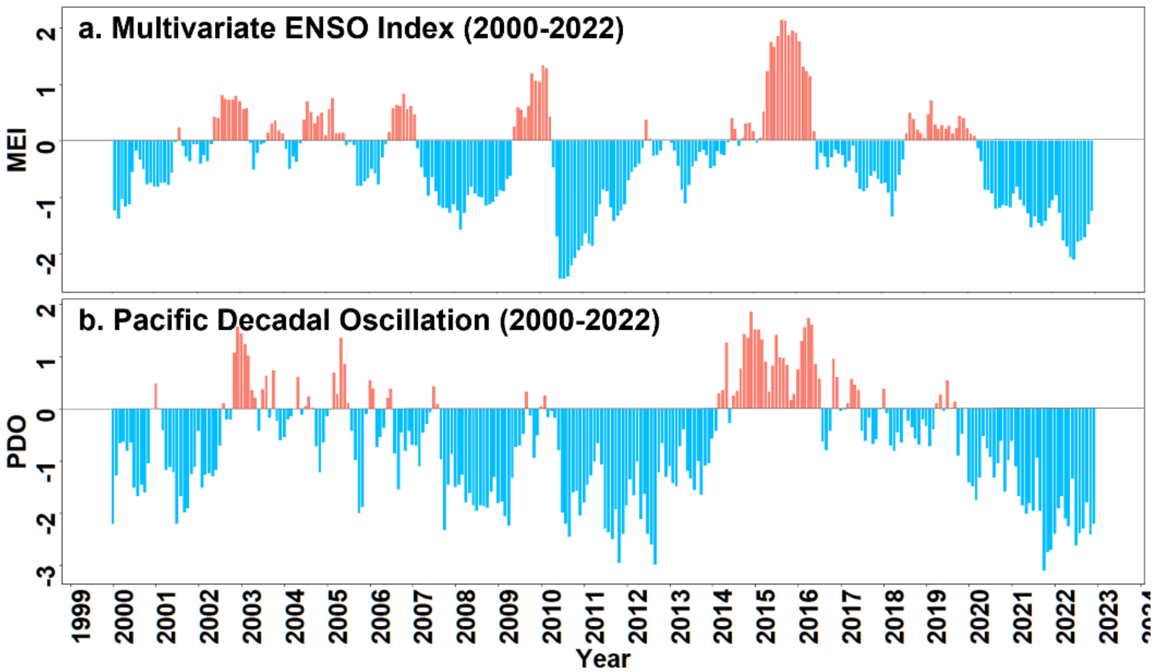

Figure 17. Multivariate ENSO Index (MEI) (a) and Pacific Decadal Oscillation Index (PDO) (b) between 2000 and 2022 (Data Source: National Centers for Environmental Information, National Oceanic and Atmospheric Administration (https://psl.noaa.gov))

*Corresponding Author: advcarrillo@gmail.com; +69612656020

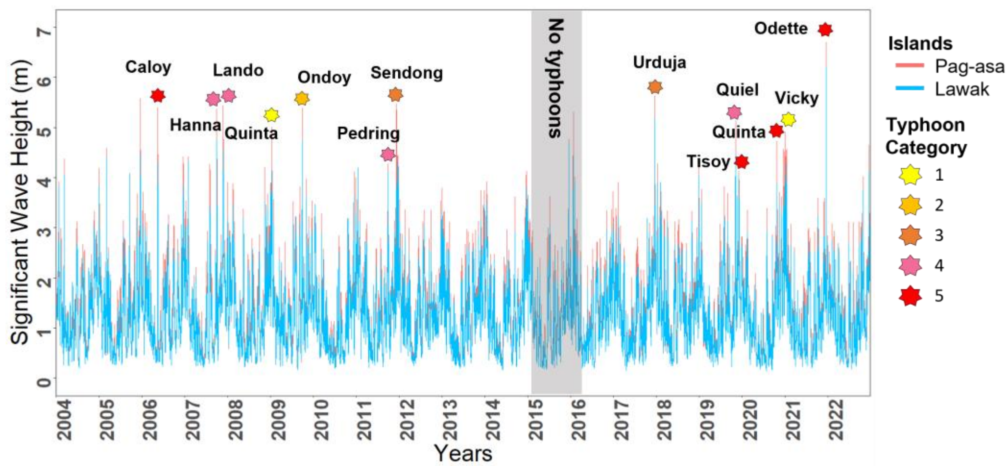

Figure 18. Peaks in significant wave height are possibly associated with storm events. (Data Sources: Copernicus Climate Change Service, Climate Data Store, Joint Typhoon Warning Center)

*Corresponding Author: advcarrillo@gmail.com; +69612656020

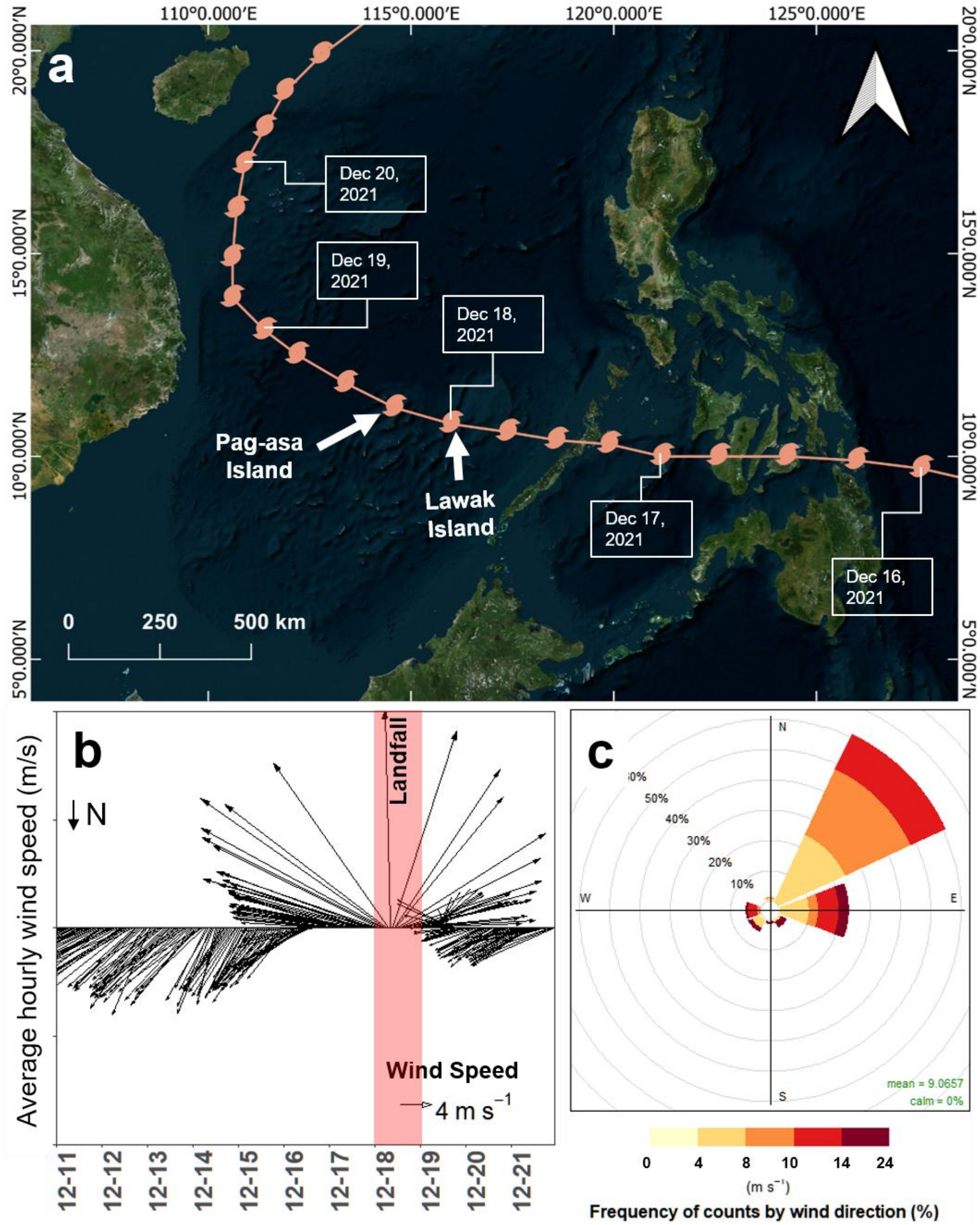

Figure 19. Tracks of Super Typhoon Odette (a) and associated wind vector (b) and wind rose diagram (c) showing wind vectors which represent the speed (length of the arrow) and direction (direction of the arrow of wind) between December 11 to 21, 2021 (Basemap source: Bing VirtualEarth, Map data © 2023 Microsoft).

*Corresponding Author: advcarrillo@gmail.com; +69612656020

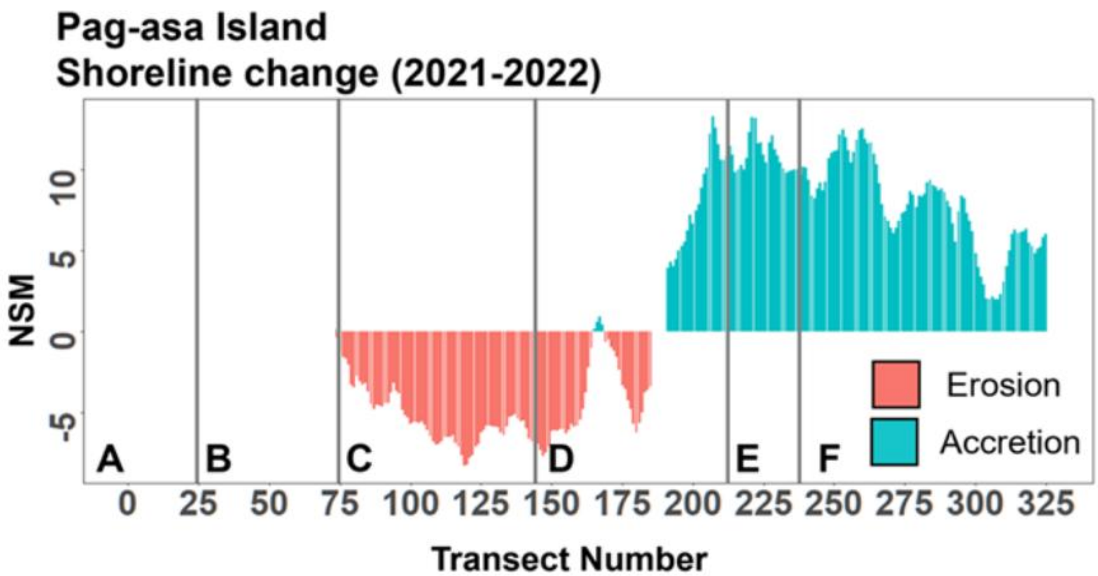

Figure 20. Net shoreline movement (NSM) for Pag-asa Island between May 2021 and February 2022 or the period before and after Super Typhoon Odette. Zones A-E are along the northern coast of Pag-asa Island while Zone F is along the southern coast. Zones A and B were excluded since these areas were affected by port construction.

*Corresponding Author: advcarrillo@gmail.com; +69612656020

Figure 21. Google Earth Image of Pag-asa Island showing white streaks of sediment traversing the reef flat from the reef crest towards the island. The tracks of sediment are most likely hidden by the seagrass beds (Image source and date: Google Earth Pro (2023), Maxar Technologies, November 29, 2016).

*Corresponding Author: advcarrillo@gmail.com; +69612656020